WARSAW UNIVERSITY OF TECHNOLOGY Index 351733
FACULTY OF CIVIL ENGINEERING
COMMITTEE FOR CIVIL AND WATER ENGINEERING
POLISH ACADEMY OF SCIENCES ISSN 1230-2945

DOI: 10.24425/ace.2025.153351

ARCHIVES OF CIVIL ENGINEERING

Vol. LXXI ISSUE 1 2025

pp. 577 –594

Research paper

Seismic energy dissipation performance of anti-buckling bracing and component composition parameters analysis

Wei Zhang[1], Lei Lv[2], Xincheng Li[3], Xinhong Ouyang[4], Zhongqiu Fu[5]

Abstract: Through the finite element method, the finite element models of three kinds of buckling-restrained brace components: cross-shaped square steel tube support, cross-shaped circular steel tube support, and circular steel tube support are established. The hysteretic performance of buckling-restrained braces under cyclic loading is analyzed, and the influence of component parameters on the mechanical performance of three kinds of buckling-restrained braces is further analyzed. The results show that the three types of buckling restrained braces have good hysteretic energy dissipation performance, and the cross-shaped square steel tube brace has the best hysteretic energy dissipation performance. The influence of the restraint stiffness ratio of the buckling-restrained brace on the mechanical properties of the three types of buckling-restrained braces is consistent. With the increase of the restraint ratio, the buckling-restrained brace reaches full-section yield. The increase of the width-thickness ratio of the inner core element will cause the yield lag of the buckling-restrained brace, while the lower width-thickness ratio of the inner core element will cause excessive stress concentration. Therefore, it is suggested that the width-thickness ratio of the inner core element should be between 5 and 10. The initial imperfection and connection stiffness of buckling-restrained braces have little effect on the bearing capacity of buckling-restrained braces.

Keywords: buckling-restrained brace, component parameters, hysteresis curve, hysteresis performance, performance analysis

[1]A.P., Department of Architecture and Civil Engineering, Zhejiang Tongji Vocational College of Science and Technology, Hangzhou, P.R. China, e-mail: zhangwei05192023@126.com, ORCID: 0009-0000-3334-1184
[2]MA.Eng, Department of Architecture and Civil Engineering, Zhejiang Tongji Vocational College of Science and Technology, Hangzhou, P.R. China, e-mail: lvlei19841125@126.com, ORCID: 0009-0007-7735-2476
[3]Ph.D. Candidate, College of Civil and Transportation Engineering, Hohai University, Nanjing, Jiangsu 210098, P.R. China, e-mail: xcxcli@foxmail.com, ORCID: 0009-0008-1171-6019
[4]MA.Eng, JSTI GROUP, Nanjing, P.R. China, e-mail: 136341737@qq.com, ORCID: 0009-0005-8678-7522
[5]Professor, College of Civil and Transportation Engineering, Hohai University, Nanjing, P.R. China, e-mail: fuzhongqiu@hhu.edu.cn, ORCID: 0009-0001-0703-1155

1. Introduction

A large number of steel-concrete arch bridges have been constructed both domestically and internationally [1]. However, inevitable accidents pose significant safety hazards to bridges, with seismic damage being particularly severe. By incorporating energy dissipation and seismic isolation structures, the bridges can effectively dissipate seismic energy and achieve a seismic reduction effect. The use of anti-buckling supports, which involve filling concrete behind the outer steel tube or directly encasing it with concrete, effectively enhances the seismic resistance of bridges [2].

A large number of studies have been conducted on the performance of flexural restraint supports. Usami et al. attempted to enhance the seismic performance of arch bridges by applying flexural restraint supports as energy dissipation dampers and numerically studied the effectiveness of Buckling-Restrained Braces (BRBs) in protecting structures against strong earthquakes [3]. Early research on flexural restraint supports was concentrated in Japan, where various forms of flexural restraint supports were developed, including concealed steel plates, external jacket restraint units, and interposed restraint units. Yoshino et al. conducted hysteresis tests on concealed steel plate shear walls [4]. Wakabayashi et al. performed a series of experimental studies on steel plate supports sandwiched between precast reinforced concrete panels, comparing the performance and hysteretic energy dissipation properties of different non-adhesive materials [5]. Kimura et al., Fujimoto et al., and Tada et al. conducted experimental studies on flexural restraint supports with rectangular steel tubes filled with mortar [6–8]. Iwata et al. compared four different types of flexural restraint supports with various cross-sections in Japan through experimental testing [9]. In the late 1990s, research and application of flexural restraint supports and their structural systems began to receive attention in the United States [10–13]. Kim et al. studied the energy dissipation capacity and seismic response of steel structures equipped with buckling-restrained braces (BRBs) and proposed a simple design method to achieve a desired displacement target [14]. Wang et al. evaluated the collapse capacity and failure mode of a skewed bridge retrofitted with flexural restraint supports (BRBs) at column flexural locations [15]. Jiang et al. used refined finite element models to assess the contact forces between core and external confinement components and studied the performance of flexural restraint supports [16]. Furthermore, the influence of the strength and stiffness of external confinement components, core length, and other geometric parameters on the performance of BRBs has been investigated. Abedini et al. employed nonlinear time history analysis to examine the performance of flexural restraint support structures under seismic excitation and conducted optimization design research [17]. Hoveidae et al. investigated the effect of repeated earthquakes on the performance of steel buckling-restrained brace frames [18]. Castaldo et al. studied the effectiveness of flexural restraint supports in seismic retrofitting of reinforced concrete (RC) buildings with masonry infill [19].

Different structural forms of buckling-restrained braces (BRBs) exhibit variations in energy dissipation capability and seismic response. In response to practical engineering needs, numerous studies have proposed novel types of BRB structures. Eatherton et al. [20] developed and experimentally validated a self-centering buckling-restrained brace, which employs a restoring mechanism using concentric tubes kept aligned with pre-tensioned shape

memory alloy rods and serves as an energy-dissipating seismic brace. Rahnavard et al. [21] introduced a precise modeling approach and provided a simple model for BRBs. They used the ABAQUS finite element program to model two full-scale BRB experimental specimens. After comparing the results of nonlinear dynamic analysis with those of the experimental specimens, they confirmed the effectiveness of these models. Iwata et al. [22] studied buckling-restrained braces that can provide stable hysteresis behavior even under high strain conditions and proposed a type of BRB with a higher cumulative plastic strain energy ratio. Naghavi et al. [23] conducted a numerical study on buckling-restrained brace frames (BRBFs) and compared them with concentrically braced frame (CBF) models. They found significant advantages in energy dissipation and ductility of the BRBF model compared to an equivalent CBF model, and the seismic response modification coefficient of the BRBF model also exhibited a larger value. Avci-Karatas et al. [24] carried out a numerical study on the hysteretic performance of BRBs with different core materials and different end connections. Obviously, anti-buckling supports with excellent energy absorption performance can effectively reduce the cost of the structure over its lifetime [25].

This study focuses on buckling-restrained braces (BRBs) and establishes finite element models for both traditional and new types of BRBs. Three categories of BRBs are simulated to analyze their load-bearing performance under cyclic loading. The hysteresis behavior of the BRBs under repeated loading is examined, followed by an analysis of the influence of different component parameters on their load-bearing performance. Finally, the seismic energy dissipation performance of the three types of BRBs is evaluated, and reasonable design suggestions for buckling-restrained braces are proposed.

2. Buckling-restrained brace seismic analysis model

2.1. Buckling-restrained brace structure

The study in this paper focuses on three types of anti-buckling supports with different cross-sections, as shown in Figure 1. In Type A, the core material is cruciform steel, and the constraint component is square steel tube filled with concrete, as shown in Figure 1(a). In Type B, the core material is cruciform steel, and the constraint component is circular steel tube filled with concrete, as shown in Figure 1(b). Type C represents a new type of anti-buckling support structure, as shown in Figure 1(c). The core material is a circular steel tube, and the constraint component is also a circular steel tube.

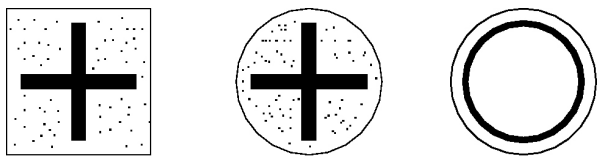

Fig. 1. Form of anti-buckling support Section: (a) A, (b) B, (c) C

2.2. Model establishment

Three finite element models of buckling-restrained braces were established using the finite element software ANSYS, as shown in Figure 2. The inner core elements all use the SOLID45 element, the outer concrete confinement for Section A and Section B uses the SOLID651 element, the steel tube uses the SHELL181 element, and the outer steel tube for Section C uses the SOLID45 element. All model target faces and contact surfaces use the TARGE170 and CONTA173 elements. Inner core element size of A, B and C section is 74×16 mm, 94×12 mm and 118×6 mm respectively. External confinement size is $150 \times 150 \times 6$ mm, 170×6 mm and 140×9 mm respectively. The A, B and C sections are respectively indicated as (a), (b) and (c) in Figure 2. Component length is 5000 mm, initial defect is 0.1%, clearance is 2 mm.

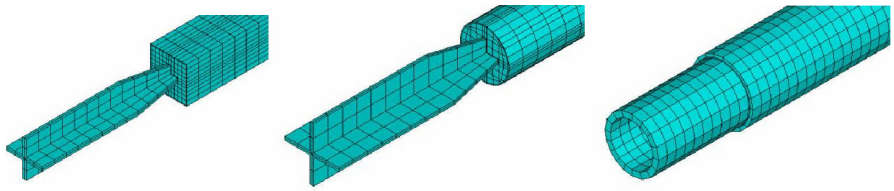

(a) (b) (c)

Fig. 2. Finite element model, Section: (a) A, (b) B, (c) C

2.3. Material configuration

This article employs the classic bilinear kinematic hardening model to simulate the constitutive relationship of the steel material. It uses the stress-strain hysteresis curve recommended by the code to simulate the constitutive relationship of concrete. The constitutive curve steel is shown in Figure 3(a).The constitutive curve of concrete is shown in Figure 3(b).

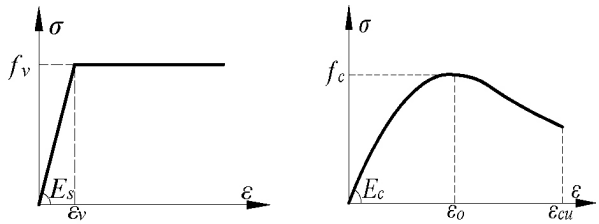

(a) (b)

Fig. 3. Constitutive curve: (a) Steel, (b) Concrete

An analysis of the hysteresis performance of the three types of buckling-restrained braces mentioned above was conducted. The inner core elements are made of Q235 steel, while the outer confinement elements are made of C30 concrete and Q345 steel, the strength of C30 concrete is 30 MPa. The selected material parameters are listed in Table 1.

Table 1. Parameters of materials related to anti-buckling supports

Material	Elastic modulus E (GPa)	Peak compressive stress f (MPa)	Peak compressive strain ε	Poisson's ratio
Q235 steel	206	235	\	0.3
Q345 steel		345		
C30 concrete	30	30	0.002	0.3

3. Analysis of hysteresis behavior of buckling-restrained braces

3.1. Load conditions

To further clarify the hysteresis behavior of the three types of buckling-restrained braces, a displacement-controlled loading system with increasing deformation amplitudes was adopted. The deformation amplitudes correspond to 1 to 10 times, 12 times, and 15 times the tensile yield deformation of the inner core component during the restrained yield segment. Each cycle was repeated three times (Figure 4). The horizontal coordinate n represents the number of cycles; The ordinate m represents the multiple of the tensile yield deformation value.

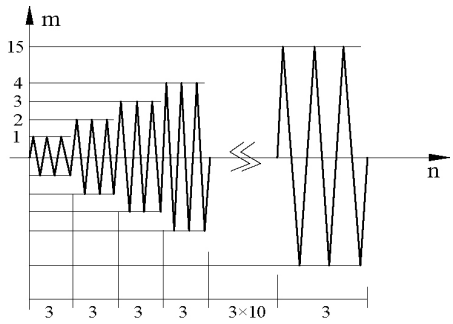

Fig. 4. Loading history

3.2. Hysteresis performance analysis

The axial hysteretic curve of the anti-buckling brace was extracted to study its anti-seismic energy absorption effect, which are presented in Figure 5. Wherein (a), (b), and (c) respectively represent the axial hysteretic curves of the three types of anti-buckling braces, A, B and C. It can be seen from the figure that the axial hysteresis curves of the three types of bracing are stable and full, indicating good energy dissipation capacity. Although lateral deformation occurs in the inner core bracing, the confinement provided by the outer casing restricts its lateral deformation, allowing the inner core bracing to only develop into higher-order buckling modes.

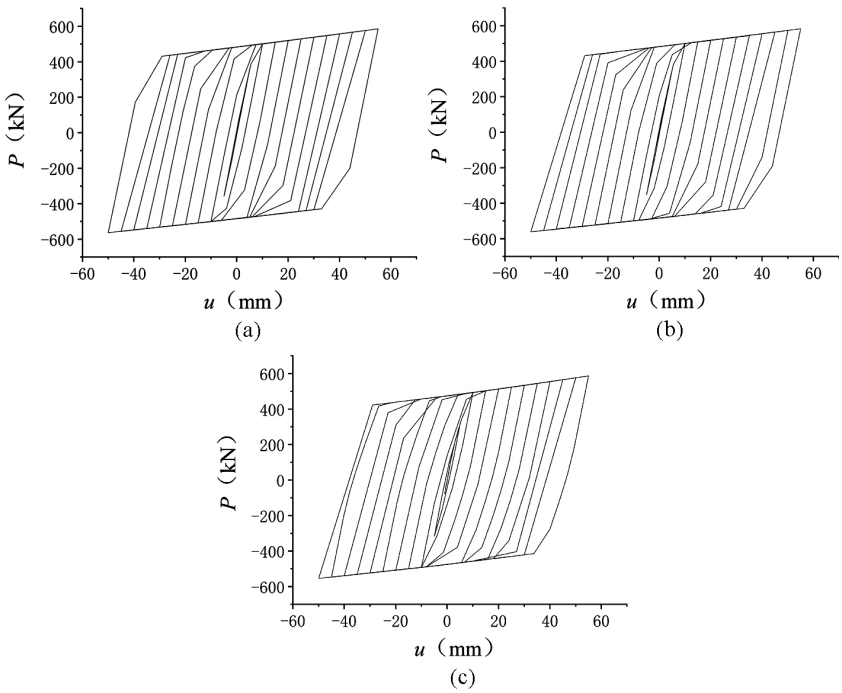

Fig. 5. Hysteresis curve, Section: (a) A, (b) B, (c) C

The comparison of the load-displacement hysteresis curves for the three types of buckling-restrained braces at the same displacement amplitude is shown in Figure 6. From the figure, it can be observed that the complete hysteresis loops of the three types of braces with the same displacement amplitude overlap significantly, with only minor differences during the unloading process after reaching the amplitude. From the numerical analysis results, it can be concluded that all three types of buckling-restrained braces exhibit good hysteresis energy dissipation performance.

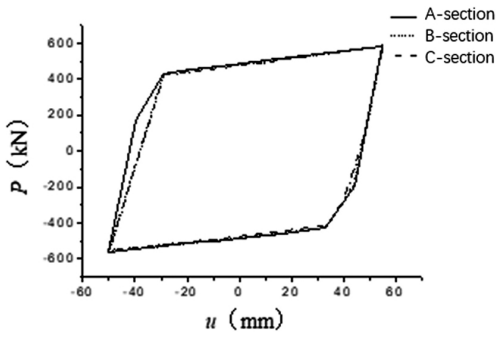

Fig. 6. Load displacement curve comparison

4. Analysis of factors influencing component composition

4.1. Constraint stiffness

The constraint stiffness is a physical quantity that describes the effectiveness of the peripheral constraint element on the core element. It is typically measured using the constraint ratio $\zeta = P_{cr.g}/F_y$. $P_{cr.g}$ is the peripheral constraint element buckles under the applied load with boundary conditions of hinged connections at both ends, $P_{cr.g} = \pi^2 E_2 I_2 / l^2$. F_y is the yield load of the core element, $F_y = A_l f_y$.

For Type A buckling-restrained brace, the dimensions of the peripheral constraint element are varied to achieve changes in the constraint stiffness ratio ζ, and compared with the yield load F_y of the core element. In the calculations, the length of the buckling-restrained brace is $l = 5000$ mm, with a gap of 2 mm, and an initial defect is assumed to be 0.1% of the component length. The composition of the brace and the calculation results are shown in Table 2.

Table 2. Composition and ultimate bearing capacity of Section A anti-buckling support

Serial number	Core element		Peripheral constraint element		ζ	P_l (kN)	$\frac{P_l}{F_y}$
	$b \times t$ (mm)	F_y (kN)	$B \times H \times T$ (mm)	$P_{cr.g}$ (kN)			
SJ1	74 × 16	496	150 × 150 × 6	1516	3.06	517.05	1.04
SJ2	74 × 16	496	150 × 130 × 6	1062	2.14	516.67	1.04
SJ3	74 × 16	496	150 × 110 × 6	704	1.42	516.39	1.04
SJ4	74 × 16	496	150 × 100 × 6	559	1.13	516.24	1.04
SJ5	74 × 16	496	130 × 100 × 6	493	0.99	516.22	1.04
SJ6	74 × 16	496	110 × 100 × 6	428	0.86	211.10	0.43
SJ7	74 × 16	496	100 × 100 × 6	395	0.80	197.20	0.40

The impact curves of the constraint ratio on load-displacement and the influence curve of the constraint ratio on the ultimate bearing capacity are shown in Figures 7 and 8, respectively. The results indicate that for SJ1~SJ5 series buckling-restrained braces, i.e., the constraint stiffness ratio $\zeta \geq 1.05$, the buckling-restrained brace's critical load P_{cr} is higher than the core element's yield load F_y. When the axial strain reaches 0.2%, the buckling-restrained brace achieves full cross-section yield, and the load-displacement curve tends to be horizontal, the compressive load Pl gradually approaches and eventually reaches the core element's compressive yield load F_y. For SJ6 and SJ7 series buckling-restrained braces, their constraint stiffness ratios are $\zeta = 0.91$ and $\zeta = 0.74$, respectively. Due to insufficient external constraint stiffness, the critical load P_{cr} is lower than the core element's yield load F_y, which causes the core element to fail in full cross-section compression before reaching yield and to buckle prematurely. When the axial strain reaches 0.2% and 1.2%, respectively, the buckling-restrained brace fails due to buckling instability, and the load-displacement curve shows a descending segment. The ultimate bearing capacities are 211.10 kN and 197.20 kN, respectively.

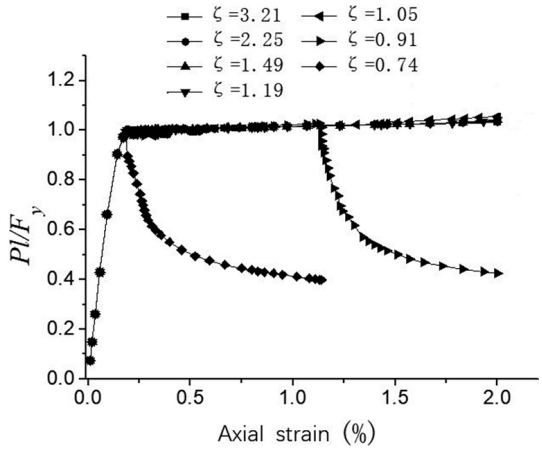

Fig. 7. The influence of constraint ratio

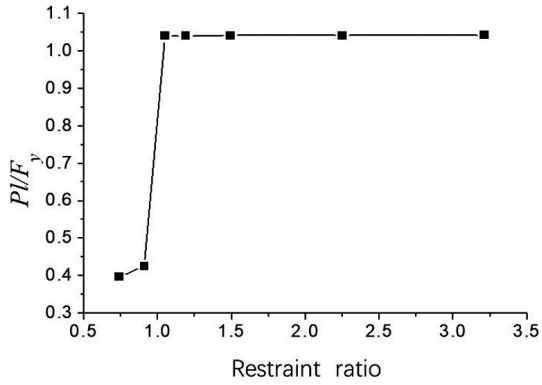

Fig. 8. Influence of ABB constraint ratio

Table 3. Composition and ultimate bearing capacity of Section B anti-buckling support

Serial number	Core element		Peripheral constraint element		ζ	P_l (kN)	$\frac{P_l}{F_y}$
	$b \times t$ (mm)	F_y (kN)	$D \times T$ (mm)	$P_{cr.g}$ (kN)			
SY1	94 × 12	496	170 × 6	1351	2.72	509.41	1.03
SY2	94 × 12	496	160 × 6	1100	2.22	509.38	1.03
SY3	94 × 12	496	150 × 6	885	1.78	509.43	1.03
SY4	94 × 12	496	140 × 6	702	1.42	508.93	1.03
SY5	94 × 12	496	130 × 6	547	1.10	508.87	1.03
SY6	94 × 12	496	120 × 6	418	0.84	222.36	0.45
SY7	94 × 12	496	110 × 6	375	0.76	176.03	0.35

For type B buckling-restrained braces, the diameter of the circular steel tube is varied to solve the bearing capacity of the buckling-restrained brace under different constraint ratios ζ. The composition of the brace and the calculation results are shown in Table 3.

The impact curves of the constraint ratio on the load-displacement curve and the effect curve of the constraint ratio on the ultimate bearing capacity are shown in Figures 9 and 10. From the graphs, it is evident that the SY series buckling-restrained braces have similar conclusions to the SJ series buckling-restrained braces. For the SY1~SY5 series buckling-restrained braces with relatively large constraint stiffness ratios ($\zeta \geq 1.10$), when the axial strain reaches 0.2%, the buckling-restrained brace achieves full cross-section yield, and the load-displacement curve tends to be horizontal, with the compressive load Pl reaching the core element's compressive yield load F_y. Conversely, for the SY6 and SY7 series buckling-restrained braces with relatively small constraint stiffness ratios ($\zeta \leq 0.84$), their critical load P_{cr} is lower than the core element's yield load F_y. The core element fails to achieve full cross-section compression yielding and buckles prematurely. When the axial strain reaches 0.2% and 0.8%, respectively, the buckling-restrained brace experiences buckling instability, and the load-displacement curve shows a descending segment. The ultimate bearing capacities are 222.36 kN and 176.03 kN, respectively.

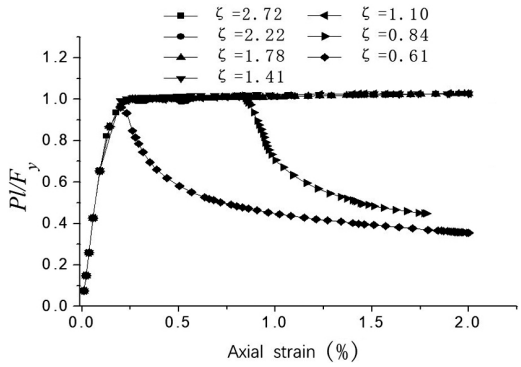

Fig. 9. Influence of ABB constraint ratio

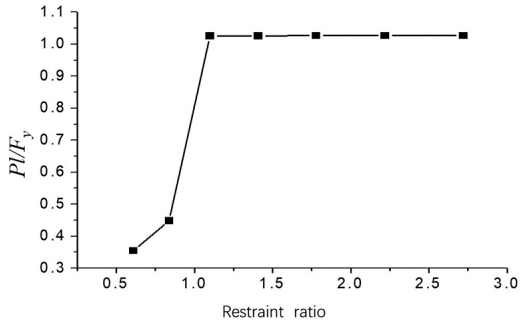

Fig. 10. Influence of ABB constraint ratio

Table 4. Composition and ultimate bearing capacity of Section C anti-buckling support

Serial number	Core element		Peripheral constraint element		ζ	P_l (kN)	$\frac{P_l}{F_y}$
	$b \times t$ (mm)	F_y (kN)	$D \times T$ (mm)	$P_{cr.g}$ (kN)			
YY1	118 × 6	496	140 × 9	919	1.85	528.09	1.06
YY2	118 × 6	496	138 × 8	833	1.68	527.82	1.06
YY3	118 × 6	496	136 × 7	751	1.51	528.17	1.06
YY4	118 × 6	496	134 × 6	672	1.36	526.08	1.06
YY5	118 × 6	496	132 × 5	597	1.20	527.87	1.06
YY6	118 × 6	496	130 × 4	526	1.06	265.70	0.54
YY7	188 × 6	496	128 × 3	457	0.92	186.84	0.38

For type C buckling-restrained braces, the core element size is $d \times t = 118 \times 6$, with a length of 5000 mm, gap of 2 mm, and initial defect of 0.1%. By varying the wall thickness of the outer constraint circular steel tube, the bearing capacity of the buckling-restrained brace is analyzed under different constraint ratios ζ. The composition of the brace and the calculation results are shown in Table 4.

Figure 11 and Figure 12 show the influence curves of the confinement ratio on the load-displacement curve of the anti-buckling support and the influence curve of the confinement ratio on the ultimate bearing capacity. For YY1~YY5 series anti-buckling supports with a confinement stiffness $\zeta \geq 1.20$, they satisfy the condition that the buckling resistance load P_{cr} is higher than the yield load F_y of the core unit. When the axial strain reaches 0.2%, the anti-buckling support reaches full cross-section yielding, and the load-displacement curve tends to be horizontal, with the compressive load Pl reaching the compressive yield load F_y of the core

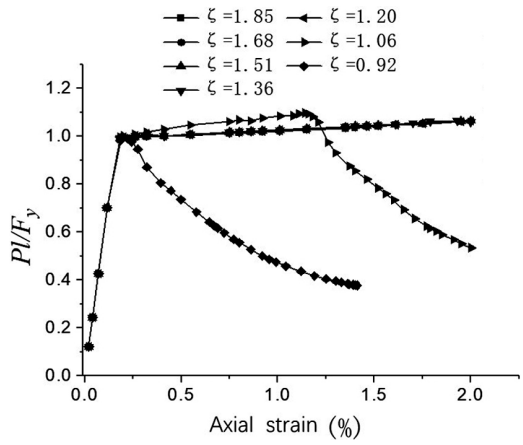

Fig. 11. Influence of constraint ratio

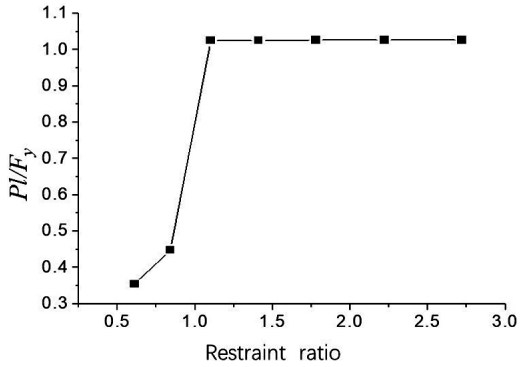

Fig. 12. Influence of ABB constraint ratio

unit. However, for YY6 and YY7 series anti-buckling supports with confinement stiffness ratios $\zeta = 1.06$ and $\zeta = 0.92$ respectively, when the axial strain reaches 0.2% and 1.2% respectively, the anti-buckling support undergoes buckling instability, and the load-displacement curve shows a descending segment, with ultimate bearing capacities of 265.70 kN and 186.84 kN respectively.

The results indicate that the influence of confinement ratio variation on the load-bearing performance of the three types of anti-buckling supports shows a consistent trend. When the confinement ratio is small, the buckling resistance load P_{cr} of the anti-buckling support is lower than the yield load F_y of the core unit, and the core unit undergoes buckling instability and loses its bearing capacity before reaching full cross-section yielding. With the increase in confinement ratio, the requirement of the buckling resistance load P_{cr} being higher than the yield load F_y of the core unit is met, and the anti-buckling support reaches full cross-section yielding. The load-displacement curve tends to be horizontal, and the compressive load Pl reaches the compressive yield load F_y of the core unit.

4.2. Width-to-thickness ratio of the core unit

The effect of different width-to-thickness ratios of the core unit on the bearing capacity of anti-buckling supports is considered. Based on Type B anti-buckling support (SY series), with a core segment length of $l = 5$ m and a gap of 2 mm. Keeping the outer confinement section size at 200×12 constant, the bearing capacity performance of the anti-buckling support under different width-to-thickness ratios of the core unit is analyzed by changing the size of the core unit plate (the size of the core unit plate is 60×20, 100×12, 150×8, respectively). The load-displacement curves are shown in Figure 13.

For the core unit plate with a larger width-to-thickness ratio of 150×8, the aspect ratio of the core unit is relatively large, resulting in a smaller relative stability coefficient. This makes the core unit plate prone to local instability. Consequently, under the same compressive load Pl, the axial strain of the core unit plate with a larger width-to-thickness ratio is larger, as shown by the smaller slope of the load-displacement curve in the figure, indicating a lower initial stiffness and axial strain greater than 0.3% when reaching full cross-section yield compared to the core

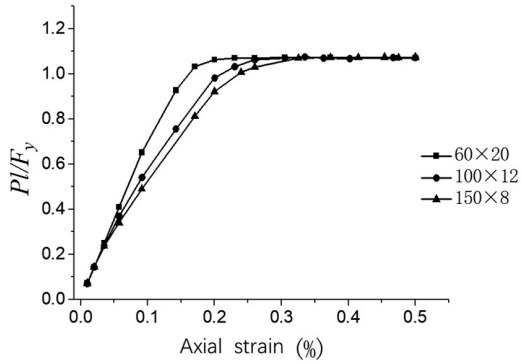

Fig. 13. Influence of width-thickness ratio on displacement curve of support load

unit plate with a smaller width-to-thickness ratio, such as 60×20, where the axial strain is 0.2% at full cross-section yield. It can be observed that with the increase in width-to-thickness ratio, the core unit experiences a certain degree of yield delay. However, after the axial strain reaches 0.3%, the load-displacement curves of the anti-buckling support components with different width-to-thickness ratios of the core unit tend to become horizontal, and the axial stress reaches the cross-section yield load F_y.

As a type of seismic energy dissipation support, the anti-buckling support exhibits better seismic energy dissipation performance with a larger hysteresis loop area under repeated loading. As shown in Figure 13, the smaller the width-to-thickness ratio of the core unit, the greater the initial elastic stiffness. Under repeated loading, the hysteresis loop is more full. In addition, seismic forces have a high strength and high frequency characteristic, requiring the anti-buckling support to have good low-cycle fatigue performance. Therefore, as mentioned above, the width-to-thickness ratio of the core unit in the anti-buckling support should not be too large. On the other hand, to meet the requirements of bolt arrangement in the connection section of the core unit, the size of the connection section should not be too small. At the same time, in order to avoid excessive stress concentration, the cross-sectional dimensions of the connection section and the core section should not differ too much. Therefore, the width-to-thickness ratio of the core plate should not be too small.

4.3. Initial defect

Due to the limitations of the manufacturing process, the anti-buckling support may have a certain initial curvature. This initial curvature causes the core unit to come into contact with the surrounding restraining unit even under a small load. Therefore, the influence of different restraint ratios on the initial defect's effect on the load-bearing performance of the anti-buckling support is considered. The SJ2 ($\zeta = 2.25$), SJ3 ($\zeta = 1.49$), and SJ5 ($\zeta = 1.05$) types of anti-buckling supports were selected for the study. The geometric initial defects were taken from the first buckling mode of the component, with respective amplitudes of 0.1%, 0.2%, and 0.5% of the longitudinal length.

Figures 14 and 15 respectively present the computed results for the SJ5 and SJ3 supports with smaller restraint ratios ($\zeta < 2.0$) under three given geometric initial defects from Table 4. From the figures, it can be seen that for the anti-buckling support SJ5 with $\zeta = 1.05$, under the condition of a 0.1% geometric initial defect, the anti-buckling support satisfies the condition of having a critical buckling load P_{cr} higher than the core unit's yield load F_y. When the axial strain reaches 0.2%, the anti-buckling support achieves full cross-section yielding, and the load-displacement curve tends to be horizontal, with the compressive load Pl reaching the core unit's compressive yield load F_y. However, under the conditions of a 0.2% and 0.5% geometric initial defect, its critical buckling load P_{cr} is lower than the core unit's yield load F_y. The core unit cannot achieve full cross-section compressive yielding and experiences premature buckling instability. When the axial strains reach 0.3% and 0.2%, respectively, the anti-buckling support experiences buckling instability, and the load-displacement curve has a downward

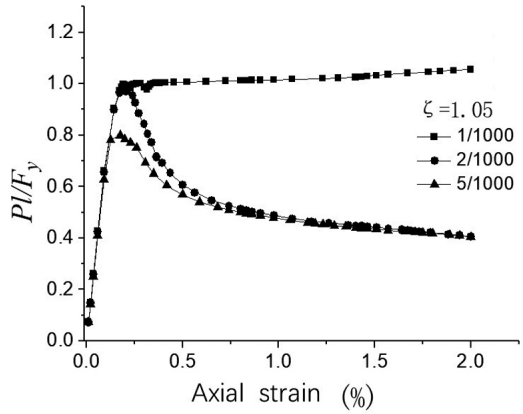

Fig. 14. Effect of initial defects

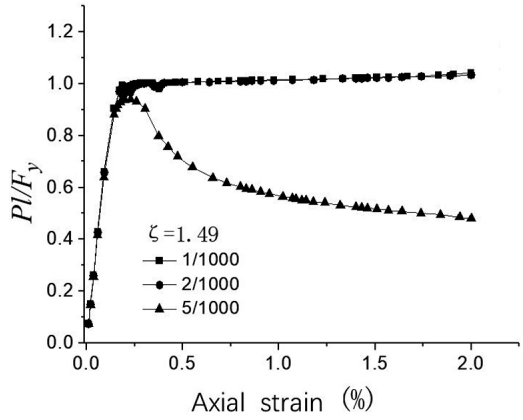

Fig. 15. Effect of initial defects

segment. Moreover, under the condition of a 0.5% geometric initial defect, the peak load of the curve is only 80% of the yield load F_y, which is 396.55 kN. For the anti-buckling support SJ3 with $\zeta = 1.49$, it satisfies the condition of having a critical buckling load P_{cr} higher than the core unit's yield load F_y under the conditions of a 0.1% and 0.2% geometric initial defect. When the axial strain reaches 0.2%, the anti-buckling support achieves full cross-section yielding, and the load-displacement curve tends to be horizontal, with the compressive load Pl reaching the core unit's compressive yield load F_y. However, under the condition of a 0.5% geometric initial defect and a compressive strain of 0.3%, the anti-buckling support experiences buckling instability, and the load-displacement curve has a downward segment. The ultimate bearing capacity is 238.18 kN.

Figure 16 presents the computed results for the anti-buckling support SJ2 with a larger restraint ratio ($\zeta > 2.0$) from Table 4. For the anti-buckling support SJ2 with a restraint ratio of $\zeta = 2.25$, full cross-section yielding can be achieved under the conditions of a 0.1%, 0.2%, and 0.5% geometric initial defect. The load-displacement curve tends to be horizontal, with the compressive load Pl reaching the core unit's compressive yield load F_y. It can be seen that as the restraint ratio increases, the influence of defects on the performance of the anti-buckling support component gradually weakens. When the restraint ratio satisfies certain conditions (restraint ratio $\zeta \geq 2.0$), the effect of geometric initial defects on the bearing capacity performance of the anti-buckling support is not significant.

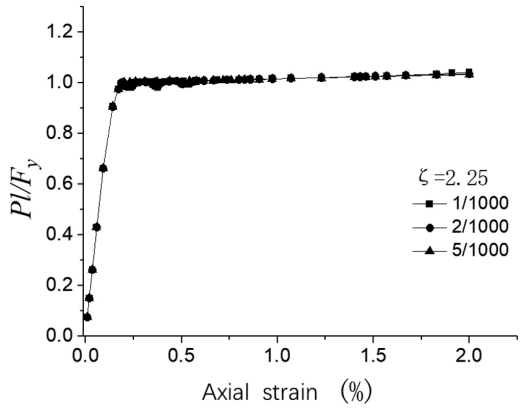

Fig. 16. Effect of initial defects on SJ2 load displacement curve

4.4. Rigid connection

The anti-buckling support only bears axial forces and cannot withstand shear and bending moments. Therefore, in general numerical analysis calculations, the connection of the support is considered as an ideal hinge. However, in practical engineering, a completely ideal hinged connection does not exist. At the same time, in order to ensure stability at the connection of the anti-buckling support, a certain level of rigidity is required. This study considers two extreme cases: ideal hinged connection and ideal rigid connection, to analyze the influence of connection rigidity on the load-carrying performance of the anti-buckling support, as shown in

Figure 17 and 18. The SJ2 ($\zeta = 2.25$) and SJ6 ($\zeta = 0.91$) types of anti-buckling supports are selected for the study. Loading mode one is axis concentrated force loading, loading mode two is cross-section uniform force loading.

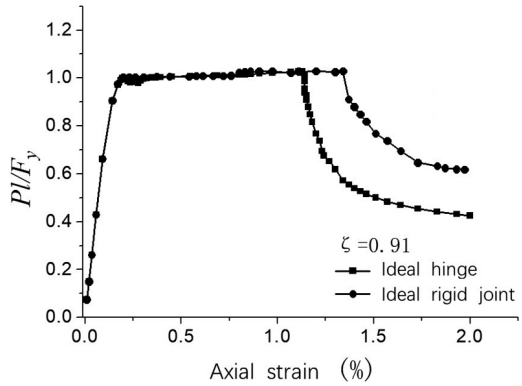

Fig. 17. Influence of connection rigidity on SJ6

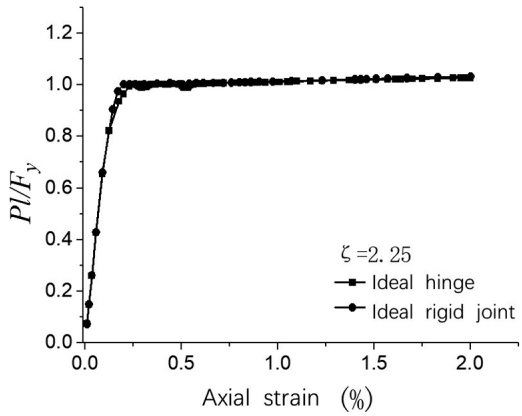

Fig. 18. Influence of connection rigidity on SJ2

From the load-displacement curves, it can be observed that for the SJ6 ($\zeta = 0.91$) anti-buckling support with relatively small restraint ratio, when an ideal rigid connection is used at the ends, its load-carrying performance is improved compared to the ideal hinged connection. The axial strain increases from 1.1% to 1.3% as the load-displacement curve descends, and the ultimate bearing capacity increases from 211.10 kN to 304.97 kN. For the SJ2 ($\zeta = 2.25$) anti-buckling support with a larger restraint ratio, both ideal rigid connection and ideal hinged connection at the ends can achieve full cross-section yielding, and the compressive load Pl can reach the yield load F_y of the core unit. Therefore, when the restraint stiffness ratio satisfies certain conditions ($\zeta \geq 2.0$), a relatively simple end connection configuration can be used for the anti-buckling support.

5. Discussions

According to the working principle of the anti-buckling brace and the influence of the component composition on the performance of the anti-buckling brace, combined with the existing research progress, the design points of the anti-buckling brace are put forward: (1) The section size of external constraint element of anti-buckling support should meet the requirement that the constraint stiffness ratio should not be less than 2.0. (2) The width to thickness ratio of the inner core plate is recommended to take 5~10. (3) The gap between the anti-buckling support inner core unit and the outer constraint unit should be less than 1/250 of the section side length of the inner core, so as to avoid the breakage of the outer constraint unit. It is generally recommended to take 1~2 mm. (4) The section size of the anti-buckling brace should meet the structural requirements of the corresponding specifications, and the additional internal force can not be ignored during the design. When the arrangement is a chevron shape, the difference of tensile and compressive internal force should be considered. (5) It is necessary to calculate the global and local stability of the anti-buckling bracing and the maximum internal force that can be generated by the connection segment.

6. Conclusions

By analyzing the hysteresis performance of three types of anti-buckling supports through finite element models, the influence of restraint stiffness ratio, core unit width-to-thickness ratio, initial defects, and connection rigidity on the load-carrying performance of the supports was calculated and analyzed. The following conclusions were drawn:

1. All three types of anti-buckling supports exhibit good hysteresis energy dissipation performance. Under the same displacement amplitude, the area enveloped by the complete hysteresis loop follows the order: Section A > Section B > Section C. It is suggested that the anti-buckling support of the real bridge should be in the form of cross-shaped square steel tube support.
2. The trend of the influence of restraint stiffness ratio variation on the load-carrying performance of the anti-buckling supports is consistent for all three types. When the restraint ratio is relatively small, the core unit does not reach full cross-section yielding before buckling instability occurs, resulting in loss of bearing capacity. As the restraint ratio increases, the anti-buckling supports achieve full cross-section yielding, and the load-displacement curve tends to be horizontal, with the compressive load Pl reaching the compressive yield load F_y of the core unit.
3. Regarding the core unit width-to-thickness ratio, an increase in this ratio leads to a certain degree of yield lag and affects the low-cycle fatigue performance of the anti-buckling supports. To meet the requirements of the connection structure of the core unit and avoid excessive stress concentration, it is recommended that the width to thickness ratio of the inner core unit of the real bridge be selected in the range of 5~10.
4. For the initial defects and connection rigidity of the anti-buckling support components, they have a significant impact on the mechanical performance of the supports when the

restraint stiffness ratio is relatively small. However, when the restraint stiffness ratio satisfies certain conditions (restraint ratio $\zeta \geq 2.0$), their influence on the load-bearing performance of the anti-buckling supports is minimal. Therefore, the constraint stiffness ratio in the design of anti-buckling bracing is 2.

References

[1] D.Y. Zhang, X. Li, W.M. Yan, W.C. Xie, and M.D. Pandey, "Stochastic seismic analysis of a concrete-filled steel tubular (CFST) arch bridge under tridirectional multiple excitations", *Engineering Structures*, vol. 52, pp. 355–371, 2013, doi: 10.1016/j.engstruct.2013.01.031.

[2] M. Iwata and M. Murai, "Buckling-restrained brace using steel mortar planks; performance evaluation as a hysteretic damper", *Earthquake Engineering & Structural Dynamics,* vol. 35, no. 14, pp. 1807–1826, 2006, doi: 10.1002/eqe.608.

[3] T. Usami, Z. Lu, and H. Ge, "A seismic upgrading method for steel arch bridges using buckling-restrained braces", *Earthquake Engineering & Structural Dynamics*, vol. 34, no. 4-5, pp. 471–496, 2005, doi: 10.1002/eqe.442.

[4] T. Yoshino and Y. Karino, "Experimental Study on Shear Wall With Braces: Part 2", in *Summaries of Technical Papers of Annual Meeting, Structural Engineering Fascicle*, vol. 11. Architectural Institute of Japan, 1971, pp. 403–404.

[5] M. Wakabayashi, T. Nakarnura, A. Kashibara, T. Morizono, and H. Yokoyama, "Experiment Study of Elastoplastic Properties of Precast Concrete Wall Panels with Built-Insulating Braces", in *Summaries of Technical Papers of Annual Meeting,* vol. 104121044. Architectural Institute of Japan, 1973, pp. 1041–1044, 1973.

[6] K. Kimura and T.Y. Takeda, "Tests on Braces Encased by Mortar In-filled Steel Tubes", in *Summaries of Technical Papers of Annual Meeting*, vol. 1041. Architectural Institute of Japan, 1976, pp. 1041–1042.

[7] M. Fujimoto, A. Wada, E. Sacki, A. Watanabe, and Y. Hitomi, "A Study on the Unbonded Steel Diagonal Braces", *Journal of Structural and Construction Engineering*, vol. 34, pp. 249–258, 1988.

[8] S. Kuwahara, M. Tada, et al., "A study on Stiffening Capacity of Double-Tube Members", *Journal of Structural and Construction Engineering*, vol. 445, pp. 151–158, 1993, doi: 10.3130/aijsx.445.0_151.

[9] M. Iwata, T. Kato, and A. Wada, "Buckling-Restrained Braces as Hysteretic Dampers", in *STESSA 2000: Behaviour of Steel Structures in Seismic Areas*. CRC Press, 2000, pp. 33–38.

[10] P. Clark, I. Aiken, K. Kasai, E. Ko, and I. Kimura, "Design Procedures for Buildings Incorporating Hysteretic Damping Devices", in *Proceedings, 69^{th} Annual Convention, Structural Engineers Association of California, Santa Barbara*, Sacramento, CA, 1999.

[11] Y. Koetaka, H. Nakamura, and O. Tsuyita, "Experimental Study on Buckling Restrained Braces", in *Proceedings of Sixth Pacific Structural Steel Conference*. Beijing, China, 2001, pp. 15–17.

[12] R. Sabelli R,S. Mahin, and C. Chang, "Seismic demands on steel braced frame building with buckling-restrained braces", *Engineering Structures*, vol. 25, no. 5, pp. 655–666, 2003, doi: 10.1016/S0141-0296(02)00175-X.

[13] J. Kim and H. Choi, "Behavior and design of structures with buckling-restrained braces", *Engineering Structures*, vol. 26, no. 6, pp. 693–706, 2004, doi: 10.1016/j.engstruct.2003.09.010.

[14] C. C. Chen, S. Y. Chen, and J. J. Liaw, "Application of low yield strength steel on controlled plastification ductile concentrically braced frames", *Canadian Journal of Civil Engineering*, vol. 28, no. 5, pp. 823–836, 2001, doi: 10.1139/l01-044.

[15] J. Kim and H. Choi, "Behavior and design of structures with buckling-restrained braces", *Engineering Structures*, vol. 26, no. 6, pp. 693–706, 2004, doi: 10.1016/j.engstruct.2003.09.010.

[16] Y. Wang, L. Ibarra, and C. Pantelides, "Collapse capacity of reinforced concrete skewed bridges retrofitted with buckling-restrained braces", *Engineering Structures*, vol. 184, pp. 99–184, 2019, doi: 10.1016/j.engstruct.2019.01.033.

[17] Z. Jiang, Y. Guo, B. Zhang, and X. Zhang, "Influence of design parameters of buckling-restrained brace on its performance", *Journal of Constructional Steel Research*, vol. 105, pp. 139–150, 2015, doi: 10.1016/j.jcsr.2014.10.024.

[18] H. Abedini, S.R.H. Vaez, and A. Zarrineghbal, "Optimum design of buckling-restrained braced frames", *Structures*, vol. 25, pp. 99–112, 2020, doi: 10.1016/j.istruc.2020.03.004.

[19] N. Hoveidae and S. Radpour, "Performance evaluation of buckling-restrained braced frames under repeated earthquakes", *Bulletin of Earthquake Engineering*, vol. 19, pp. 241–262, 2021, doi: 10.1007/s10518-020-00983-0.

[20] P. Castaldo, E. Tubaldi, F. Selvi, and L. Gioiella, "Seismic performance of an existing RC structure retrofitted with buckling restrained braces", *Journal of Building Engineering*, vol. 33, 2020, doi: 10.1016/j.jobe.2020.101688.

[21] M.R. Eatherton, L.A. Fahnestock, and D.J. Miller, "Computational study of self-centering buckling-restrained braced frame seismic performance", *Earthquake Engineering & Structural Dynamics,* vol. 43, no. 13, pp. 1897–1914, 2014, doi: 10.1002/eqe.2428.

[22] R. Rahnavard, M. Naghavi, M. Aboudi, and M. Suleiman, "Investigating modeling approaches of buckling-restrained braces under cyclic loads", *Case Studies in Construction Materials,* vol. 8, pp. 476–488, 2018, doi: 10.1016/j.cscm.2018.04.002.

[23] M. Iwata, M. Midorikawa, and K. Koyano, "Buckling-restrained brace with high structural performance", *Steel construction*, vol. 11, no. 1, pp. 3–10, 2018, doi: 10.1002/stco.201810006.

[24] M. Naghavi, R. Rahnavard, R.J. Thomas, and M. Malekinejad, "Numerical evaluation of the hysteretic behavior of concentrically braced frames and buckling restrained brace frame systems", *Journal of Building Engineering,* vol. 22, pp. 415–428, 2019, doi: 10.1016/j.jobe.2018.12.023.

[25] C. Avci-Karatas, O.C. Celik, and S.O. Eruslu, "Modeling of buckling restrained braces (BRBs) using full-scale experimental data", *KSCE Journal of Civil Engineering*, vol. 23, no. 10, pp. 4431–4444, 2019, doi: 10.1007/s12205-019-2430-y.

[26] D. Wieczorek, K. Zima and E. Plebankiewicz, "Expert studies on the impact of risk on the life cyclecosts of buildings", *Archives of Ciyil Engineering*, vol. 69, no. 4, pp. 105–123, 2023, doi: 10.24425/ace.2023.147650.

Received: 2023-12-12, Revised: 2024-04-23